

An Adaptive Nonlinear Sensorless Controller of Doubly Fed Induction Generator Driven By Wind Turbine

Radouane Ourhdir*, Mohammed Rachidi

Department of Electromechanical Engineering, Ecole Nationale Supérieure des Arts et Métiers, Moulay Ismail university, Meknès, BP 4024, Morocco

ARTICLE INFO

Article history:

Received: 01 July, 2020

Accepted: 07 September, 2020

Online: 20 November, 2020

Keywords:

Doubly fed induction generator (DFIG)

Control Wind Power Generation

Rotor speed observer

Unknown Aerodynamic Torque

Unknown Rotor Winding

Resistance

Adaptive control projection operator

Lyapunov Theory

ABSTRACT

In this study, an adaptive nonlinear sensorless controller for doubly fed induction generator (DFIG) driven by a wind turbine is proposed. The aim is to maximize the extracted power by tracking the wind turbine optimal torque-speed characteristic without the need for rotor speed measurement. This controller ensures a satisfactory tracking of both stator flux and rotor speed. It considers the detailed model of DFIG in an arbitrary ($d-q$) rotating frame without any simplifying assumption. An observer provides the rotor speed estimation incorporated in the control loop. To guarantee the system stability under parametric uncertainties like the aerodynamic torque and the rotor winding resistance, which harms the efficiency and the robustness of the controller, update laws are established to estimate the uncertain parameters. Lyapunov's theory is used to prove the system stability. The proposed adaptive sensorless controller validity is demonstrated by simulation in Matlab/Simulink environment. The robustness of the controller is confirmed by the comparison between the same controller with and without adaptation.

1. Introduction

Recently, using wind energy to produce electricity has been gradually grabbing the attention of many researchers, thanks to its cleanliness and dependability. Because of its smaller power electronic components rating and its wide speed operation range, the DFIG is seen as the most used wind turbine generator [1–3]. The DFIG rotor windings are connected to the electrical grid via rotor and grid side converters (RSC and GSC) and RL filter, whereas the stator windings are immediately related to the electrical grid as illustrated by Figure 1. In the last decade, many researchers giving much focus and interest to the field of sensorless control of DFIG-based wind turbine (DFIG-WT)[4–7]. In this control strategy, the DFIG-WT systems operate without the need to use the speed sensor, which lowers the whole system cost and enhance its overall reliability by minimizing the number of components that are susceptible to failure.

There has been some research about sensorless control using proportional-integral (PI) loops such as [8,9]. The latter mainly relied on assumptions that the flux or stator voltages are constant, and the stator resistance is negligible. However, these assumptions

are useless under grid faults or load variations. Furthermore, the small resistance of the stator may cause an incorrect damped dynamics of the stator flux [10].

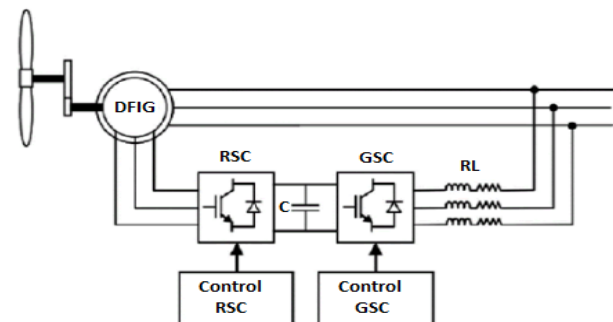


Figure 1: Schematic representation of grid connected DFIG-WT system

For the most control strategies, if the actual values do not correspond to the parameters and variables of DFIG-WT used in the control law, it could result in a failure of the closed-loop control. So, when some parameters and variables are difficult to be measured, some strategies based on estimation theory are important to generate a pertinent control. The frequency, the

*Corresponding Author: Radouane Ourhdir, radouane.ourhdir@edu.umi.ac.ma

temperature and the magnetic saturation may cause the change of DFIG parameters [11]. Therefore, the online parameter estimation or disturbance observer is compulsory to have high precision control.

Much research has addressed the control of DFIGs during parameter variation [12–14]. On the other hand, the modeling and the control of WT is not an easy task, particularly when large scale WTs, in megawatts, are considered [15,16]. Hopefully, to minimize the drive train vibration and to develop the quality of the extracted power, some works use the estimation theory in order to take into consideration the uncertainties arose from the aerodynamic torque, particularly in the stage of the maximum power point tracking (MPPT) [17].

The main focus of this work is to elaborate an adaptive sensorless control for the rotor side converter (RSC), this controller takes into consideration the detailed model of DFIG. Update laws in real-time are established to deal with the parameter uncertainties. To preserve the objectives of the MPPT without the need to use rotor speed sensor, a speed observer is incorporated in this controller. The remaining of this research paper displays as follows: The second section revolves around the model of the DFIG-WT system. The third section puts forward the suggested nonlinear controller: For the start, we present the proposed rotor speed observer. Afterward, we introduce our sensorless controller design, and we point out to the control laws of DFIG, and update laws for the speed observer, as well as the estimated rotor resistance and aerodynamic torque, which are computed using the Lyapunov theory. The last section considers simulation results and discussion. At last, we wrap up by drawing some concluding remarks.

2. DFIG-WT model

2.1. Wind turbine model

Based on wind turbine aerodynamic[18], The power captured from the wind can be expressed as :

$$P_t = \frac{1}{2} \rho \pi R^2 C_p(\lambda, \beta) v^3 \quad (1)$$

where ρ is the air density, R is the blade radius and v is the wind speed. The wind power coefficient $C_p(\lambda, \beta)$ depends on the design the blades; is a function of pitch angle β and tip speed ratio λ (TSR).

where:

$$\lambda = \frac{R \omega}{G v} \quad (2)$$

In which ω is the mechanical generator speed and G is the gearbox ratio. In the basis of the wind turbine design [18], the expression of power coefficient is:

$$C_p(\lambda, \beta) = c_1 \left(\frac{c_2}{\lambda_i} - c_3 \beta - c_4 \right) \exp\left(-\frac{c_5}{\lambda_i}\right) + c_6 \lambda \quad (3)$$

where:

$$\frac{1}{\lambda_i} = \frac{1}{\lambda + 0.08\beta} - \frac{0.035}{\beta^3 + 1}$$

The coefficients c_1 - c_6 are listed in Table 1.

Table 1: Values of coefficients c_1 - c_6

c_1	c_2	c_3	c_4	c_5	c_6
0.5176	116	0.4	5	21	0.0068

When the pitch angle β remains unchanged, there is an optimum tip ratio $\lambda = \lambda_{opt}$ that maximizes the power coefficient C_p , In this study, we assume that $\beta = 0$. So the MPPT is achieved by the control of the generator speed. Conforming to (2) the mechanical speed that optimize the extracted power is:

$$\omega^* = \frac{G \lambda_{opt}}{R_t} v \quad (4)$$

2.2. Induction generator model

Employing the flux-linkage and voltage equations of the induction generator [19], the state variables of DFIG in an arbitrary reference frame rotating at speed ω_0 include d-q rotor currents and stator fluxes $i_{dr}, i_{qr}, \varphi_{ds}, \varphi_{qs}$, and generator speed ω . The considered 5th-order state-space representation of DFIG can be expressed as:

$$\begin{cases} \frac{d\varphi_{ds}}{dt} = u_{ds} - \alpha\varphi_{ds} + \omega_0\varphi_{qs} + \alpha M i_{dr} \\ \frac{d\varphi_{qs}}{dt} = u_{qs} - \alpha\varphi_{qs} - \omega_0\varphi_{ds} + \alpha M i_{qr} \\ \frac{di_{dr}}{dt} = \frac{1}{\sigma} u_{dr} - \frac{R_r}{\sigma} i_{dr} - \alpha\beta M i_{dr} + (\omega_0 - \omega)i_{qr} \\ \quad - \beta u_{ds} + \alpha\beta\varphi_{ds} - \beta\omega\varphi_{qs} \\ \frac{di_{qr}}{dt} = \frac{1}{\sigma} u_{qr} - \frac{R_r}{\sigma} i_{qr} - \alpha\beta M i_{qr} - (\omega_0 - \omega)i_{dr} \\ \quad - \beta u_{qs} + \alpha\beta\varphi_{qs} + \beta\omega\varphi_{ds} \\ \frac{d\omega}{dt} = -\frac{f}{J} \omega + \frac{T_t}{J} - \mu(\varphi_{qs}i_{dr} - \varphi_{ds}i_{qr}) \end{cases} \quad (5)$$

with:

$$\sigma = L_r \left(1 - \frac{M^2}{L_r L_s} \right), \quad \beta = L_r \frac{M}{\sigma L_s}, \quad \mu = \frac{M}{J L_s}, \quad \alpha = \frac{R_s}{L_s}$$

T_t is the mechanical torque. The rest of the parameters of DFIG-WT system are given in Table 2, Appendix B.

3. Control design

3.1. Speed observer

Achievement of MPPT strategy requires a quick convergence of the mechanical rotor speed to its optimal value. An observer is proposed to estimate the actual rotor speed of DFIG.

$$\dot{\hat{\omega}} = -\frac{f}{J} \hat{\omega} + \frac{\hat{T}_t}{J} - \mu(\varphi_{qs}i_{dr} - \varphi_{ds}i_{qr}) + \eta \quad (6)$$

Measurement of the rotor currents and the stator fluxes are compulsory for the latter observer; it relies also on the estimated aerodynamic torque \hat{T}_t and the term η which will be elaborated by the means of the Lyapunov approach.

3.2. Reference Signals

Supposing that; the d-q rotating frame is aligned with the stator flux vector as in [20]. In our case, we consider that the stator flux vector is associated with the d-axis of the d-q reference frame giving:

$$\varphi_{qs} = 0; \varphi_{ds} = \Psi^* \quad (7)$$

Based on the assumption (7) illustrated by Figure 2, the expressions of the reference signals in the steady-state condition of DFIG can be established:

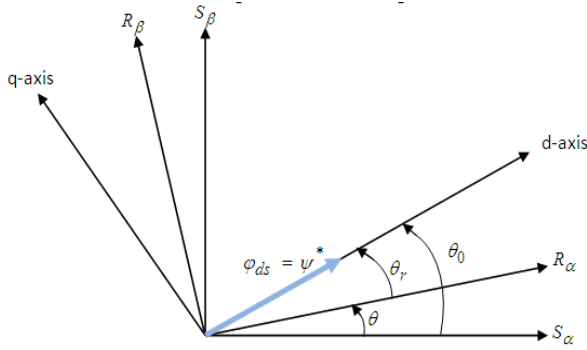


Figure 2: Determination of angles for the DFIG in d-q reference frame

Taking into consideration the latter assumption (7), and according to the first equation of (5), the reference of the direct rotor current can be expressed as follows:

$$i_{dr}^* = \frac{\Psi^*}{M} - \frac{u_{ds}}{\alpha M} + \frac{1}{\alpha M} \frac{d\Psi^*}{dt} \quad (8)$$

From the 5th equation of the system (5), the reference of the quadratic rotor current is established by replacing the aerodynamic torque by its estimate and incorporating a feedback saturation function [21], which relies on the estimated and reference rotor speed:

$$i_{qr}^* = \frac{1}{\mu\Psi^*} \left(-k_{\omega} \text{sat}(\hat{\omega} - \omega^*) + \frac{f}{J} \omega^* - \frac{\hat{T}_t}{J} + \frac{d\omega^*}{dt} \right) \quad (9)$$

where:

$$\text{sat}(y) = \begin{cases} 0.1 & \text{if } y \geq 0.1 \\ y & \text{if } -0.1 < y < 0.1 \\ -0.1 & \text{if } y \leq -0.1 \end{cases}$$

The saturation function $\text{sat}(y)$ has a finite limit at infinity; it is a linear, odd, and differentiable function in a neighborhood of the origin. To satisfy the assumption (7), the d-q reference frame must rotate at a specific speed ω_0 which is expressed using the second equation of (5):

$$\omega_0 = \dot{\theta}_0 = \frac{u_{qs} + \alpha M i_{qr}^*}{\Psi^*} \quad (10)$$

3.3. Control and update laws

The rotor speed sensor has some weak points concerning robustness, maintenance, cost, and cables linking the speed sensor and the control block. Any incorrect value provided by the rotor speed sensor may significantly harm the defined control targets

and it can also destroy the system stability. Besides, accurate modeling of the aerodynamic torque is not an easy task, and the rotor winding resistance may vary up during operation due to the heating of the generator. That is to say that it constitutes uncertain parameters for the model which can affect the system stability. Yet, to ensure the system stability and maintain the control objectives in the presence of uncertainties and without needing to measure the rotor speed, the system closed-loop stability is examined to extract the expressions of the additional term η used in the speed observer, and the update laws of the estimated rotor resistance and aerodynamic torque. In this study, we assume that the aerodynamic torque and rotor resistance are unknown and vary slowly with time and should be estimated. To this purpose, the error variables can be introduced as follows:

$$\begin{cases} \tilde{\omega} = \omega - \omega^* \\ \tilde{\varphi}_{ds} = \varphi_{ds} - \Psi^* \\ \tilde{\varphi}_{qs} = \varphi_{qs} \\ \tilde{i}_{dr} = i_{dr} - i_{dr}^* \\ \tilde{i}_{qr} = i_{qr} - i_{qr}^* \\ e_{\omega} = \hat{\omega} - \omega \\ \tilde{R}_r = R_r - \hat{R}_r \\ \tilde{T}_t = T_t - \hat{T}_t \end{cases} \quad (11)$$

Using equations (5), (6), (7), (8), (9), (10) and (11) the system of the error dynamics can be expressed as follows:

$$\begin{cases} \dot{\tilde{\varphi}}_{ds} = -\alpha \tilde{\varphi}_{ds} + \omega_0 \tilde{\varphi}_{qs} + \alpha M \tilde{i}_{dr} \\ \dot{\tilde{\varphi}}_{qs} = -\alpha \tilde{\varphi}_{qs} - \omega_0 \tilde{\varphi}_{ds} + \alpha M \tilde{i}_{qr} \\ \dot{\tilde{i}}_{dr} = \frac{u_{dr}}{\sigma} - \frac{R_r}{\sigma} i_{dr} - \alpha \beta M i_{dr} + (\omega_0 - \omega) i_{qr} \\ \quad - \beta u_{ds} + \alpha \beta \varphi_{ds} - \beta \omega \varphi_{qs} - \frac{di_{dr}^*}{dt} \\ \dot{\tilde{i}}_{qr} = \frac{u_{qr}}{\sigma} - \frac{R_r}{\sigma} i_{qr} - \alpha \beta M i_{qr} - (\omega_0 - \omega) i_{dr} \\ \quad - \beta u_{qs} + \alpha \beta \varphi_{qs} + \beta \omega \varphi_{ds} - \frac{di_{qr}^*}{dt} \\ \dot{\tilde{\omega}} = -\frac{f}{J} \tilde{\omega} + \frac{\tilde{T}_t}{J} - \mu \tilde{\varphi}_{qs} i_{dr} + \mu \tilde{\varphi}_{ds} i_{qr} + \mu \Psi^* \tilde{i}_{qr} \\ \dot{e}_{\omega} = -\frac{f}{J} e_{\omega} - \frac{\tilde{T}_t}{J} + \eta \end{cases} \quad (12)$$

In order to have a compact error dynamic system, the error variables e_d and e_q are considered instead of \tilde{i}_{dr} and \tilde{i}_{qr} :

$$\begin{cases} e_d = \tilde{\varphi}_{ds} + \frac{\tilde{i}_{dr}}{\beta} \\ e_q = \tilde{\varphi}_{qs} + \frac{\tilde{i}_{qr}}{\beta} \end{cases} \quad (13)$$

The error dynamics in (12) becomes:

$$\begin{cases} \dot{\tilde{\varphi}}_{ds} = -(\alpha + \alpha\beta M)\tilde{\varphi}_{ds} + \omega_0\tilde{\varphi}_{qs} + \alpha\beta M e_d \\ \dot{\tilde{\varphi}}_{qs} = -(\alpha + \alpha\beta M)\tilde{\varphi}_{qs} - \omega_0\tilde{\varphi}_{ds} + \alpha\beta M e_q \\ \dot{e}_d = \frac{u_{rd}}{\beta\sigma} - \frac{\tilde{R}_r}{\beta\sigma} i_{dr} + \left(\varphi_{qs} + \frac{i_{qr}}{\beta}\right) e_\omega + \eta_{0d} \\ \dot{e}_q = \frac{u_{rq}}{\beta\sigma} - \frac{\tilde{R}_r}{\beta\sigma} i_{qr} - \left(\varphi_{ds} + \frac{i_{dr}}{\beta}\right) e_\omega + \eta_{0q} \\ \dot{e}_\omega = \frac{f}{J} e_\omega - \frac{\tilde{T}_t}{J} + v \end{cases} \quad (14)$$

where:

$$\begin{aligned} \eta_{0d} &= -\frac{\hat{R}_r}{\beta\sigma} i_{dr} - \alpha M i_{dr}^* + (\omega_0 - \hat{\omega}) \frac{i_{qr}}{\beta} - (\hat{\omega} - \omega_0) \varphi_{qs} \\ &\quad + \alpha \Psi^* - u_{ds} - \frac{1}{\beta} \left(\frac{\dot{\Psi}^*}{M} - \frac{1}{\alpha M} \frac{du_{sd}}{dt} + \frac{1}{\alpha M} \frac{d^2\Psi^*}{dt^2} \right) \\ \eta_{0q} &= -\frac{\hat{R}_r}{\beta\sigma} i_{qr} - \alpha M i_{qr}^* - (\omega_0 - \hat{\omega}) \frac{i_{dr}}{\beta} + (\hat{\omega} - \omega_0) \varphi_{ds} + \omega_0 \Psi^* \\ &\quad - u_{qs} - \frac{1}{\beta} \left[-\frac{\dot{\Psi}^*}{\mu\Psi^{*2}} \left(-k_\omega \text{sat}(\hat{\omega} - \omega^*) + \frac{f}{J} - \frac{\hat{T}_t}{J} + \omega^* \right) \right. \\ &\quad \left. + \frac{1}{\mu\Psi^*} \left(-k_\omega \frac{d}{dt} \text{sat}(\hat{\omega} - \omega^*)(\hat{\omega} - \omega^*) + \frac{f}{J} \omega^* - \frac{\hat{T}_t}{J} + \dot{\omega}^* \right) \right] \end{aligned}$$

The expression of the stator direct voltage derivative $\frac{du_{sd}}{dt}$ is detailed in Appendix A. we construct a Lyapunov function for the system (14) as:

$$V = \frac{1}{2} (\tilde{\varphi}_{ds}^2 + \tilde{\varphi}_{qs}^2 + z_d^2 + z_q^2) + \frac{1}{2} \lambda e_\omega^2 + \frac{\gamma}{J} e_\omega \tilde{T}_t + \frac{\gamma^2}{\lambda J^2} \tilde{T}_t^2 + \frac{1}{2} \delta \tilde{R}_r^2 \quad (15)$$

where λ , γ and δ are positive design parameters given in Appendix B. The derivative of V along with the time gives

$$\begin{aligned} \dot{V} &= -\alpha [\tilde{\varphi}_{ds}^2 + \tilde{\varphi}_{qs}^2] - \alpha M \beta [\tilde{\varphi}_{ds}^2 + \tilde{\varphi}_{qs}^2] + \alpha M \beta [e_d \tilde{\varphi}_{ds} + z_q \tilde{\varphi}_{qs}] \\ &\quad + \tilde{T}_t \left[v \frac{\gamma}{J} - \frac{2\gamma^2}{\lambda J^2} \hat{T}_t \right] + \tilde{R}_r \left[-\frac{e_d i_{dr}}{\sigma\beta} - \frac{z_q i_{qr}}{\sigma\beta} - \delta \hat{R}_r \right] \\ &\quad + e_\omega \left[e_d \left(\varphi_{qs} + \frac{i_{qr}}{\beta} \right) - e_q \left(\varphi_{ds} + \frac{i_{dr}}{\beta} \right) + \lambda v - \frac{\gamma}{J} \hat{T}_t \right] \\ &\quad + z_q \left[\eta_{0q} + \frac{u_{qr}}{\sigma\beta} \right] + z_d \left[\eta_{0d} + \frac{u_{dr}}{\sigma\beta} \right] \\ &\quad - \frac{\lambda f}{J} e_\omega^2 - \frac{\gamma}{J^2} \tilde{T}_t^2 - \left[\frac{\lambda}{J} + \frac{f}{J^2} \right] \tilde{T}_t e_\omega \end{aligned} \quad (16)$$

It's obvious that:

$$\left(\frac{e_d}{2} - \varphi_{ds} \right)^2 + \left(\frac{e_q}{2} - \varphi_{qs} \right)^2 \geq 0 \quad (17)$$

From (17), we can get the following inequality:

$$\left[-\tilde{\varphi}_{ds}^2 - \tilde{\varphi}_{qs}^2 + e_d \tilde{\varphi}_{ds} + e_q \tilde{\varphi}_{qs} \right] \leq \frac{e_d^2 + e_q^2}{4} \quad (18)$$

The control laws are derived as:

$$\begin{cases} u_{dr} = -\sigma\beta \left[\frac{\alpha M \beta}{4} e_d + \eta_{0d} + k e_d \right] \\ u_{qr} = -\sigma\beta \left[\frac{\alpha M \beta}{4} e_q + \eta_{0q} + k e_q \right] \end{cases} \quad (19)$$

We define the dynamics of the rotor resistance as

$$\dot{\hat{R}}_r = \text{Pr oj} \left[-\frac{1}{\delta} \left[\frac{e_d i_{dr} + e_q i_{qr}}{\sigma\beta} \right], \hat{R}_r \right] \quad (20)$$

where $\text{Pr oj}[g, \hat{R}_r]$ is the projection algorithm[22], which is specified in our case by

$$\dot{\hat{R}}_r = \begin{cases} g & \text{if } R_{rM} \leq \hat{R}_r \leq R_{rm} \\ g & \text{if } \hat{R}_r < R_{rm} \text{ and } g \geq 0 \\ g & \text{if } \hat{R}_r > R_{rM} \text{ and } g \leq 0 \\ g \left[1 - \frac{R_{rM}^2 - \hat{R}_r^2}{R_{rm}^2 - (R_{rM} - \varepsilon_1)^2} \right] & \text{if } \hat{R}_r < R_{rm} \text{ and } g < 0 \\ g \left[1 - \frac{\hat{R}_r^2 - R_{rM}^2}{(R_{rM} + \varepsilon_1)^2 - R_{rM}^2} \right] & \text{if } \hat{R}_r > R_{rM} \text{ and } g > 0 \end{cases} \quad (21)$$

with R_{rM} and R_{rm} are the upper and the lower bound values of R_r , respectively, and ε_1 is an arbitrary positive constant such that $R_{rm} - \varepsilon_1 \geq 0$.

We define the update laws of the additional term and the aerodynamic torque as

$$\eta = \begin{cases} \zeta = \frac{2}{\lambda} \left[e_q \left(\varphi_{ds} + \frac{i_{dr}}{\beta} \right) - e_d \left(\varphi_{qs} + \frac{i_{qr}}{\beta} \right) \right] & \text{if } \hat{T}_t \leq T_{tM} \\ \zeta = \frac{2}{\lambda} \left[e_q \left(\varphi_{ds} + \frac{i_{dr}}{\beta} \right) - e_d \left(\varphi_{qs} + \frac{i_{qr}}{\beta} \right) \right] & \text{if } \hat{T}_t > T_{tM} \\ \frac{\zeta}{1 + P(\hat{T}_t)} & \text{and } \frac{dP(\hat{T}_t)}{dt} \zeta \leq 0 \\ \zeta & \text{Otherwise} \end{cases} \quad (22)$$

$$\dot{\hat{T}}_t = \begin{cases} \chi = \frac{J}{\gamma} \left[e_q \left(\varphi_{ds} + \frac{i_{dr}}{\beta} \right) - e_d \left(\varphi_{qs} + \frac{i_{qr}}{\beta} \right) \right] & \text{if } \hat{T}_t \leq T_{tM} \\ \chi = \frac{J}{\gamma} \left[e_q \left(\varphi_{ds} + \frac{i_{dr}}{\beta} \right) - e_d \left(\varphi_{qs} + \frac{i_{qr}}{\beta} \right) \right] & \text{if } \hat{T}_t > T_{tM} \\ \frac{1 + P(\hat{T}_t)}{1 + P(\hat{T}_t)} \chi & \text{and } \frac{dP(\hat{T}_t)}{dt} \chi \leq 0 \\ \chi & \text{Otherwise} \end{cases} \quad (23)$$

where:

$$P(\hat{T}_t) = \frac{\hat{T}_t^2 - T_{tM}^2}{2\varepsilon_2 \hat{T}_t + \varepsilon_2^2} \quad (24)$$

with T_{tM} is the upper bound value of T_t and ε_2 is an arbitrary positive constant. Substituting (18), (19), (21), (22) and (23) in (16), the time derivative of (15) becomes:

$$\dot{v} \leq -\alpha(\tilde{\varphi}_{ds}^2 + \tilde{\varphi}_{qs}^2) - \left[k - \frac{\alpha\beta M}{4} \right] (e_d^2 + e_q^2) - \lambda \frac{f}{J} e_\omega^2 - \left(\frac{\lambda}{J} + \gamma \frac{f}{J^2} \right) \tilde{T}_t e_\omega - \frac{\gamma}{J^2} \tilde{T}_t^2 \quad (25)$$

The time derivative of (15) can be written in the following way:

$$\dot{v} \leq -\min\{\alpha, C\}(\tilde{\varphi}_{ds}^2 + \tilde{\varphi}_{qs}^2 + e_d^2 + e_q^2) - \lambda \frac{f}{J} e_\omega^2 - \left(\frac{\lambda}{J} + \gamma \frac{f}{J^2} \right) \tilde{T}_t e_\omega - \frac{\gamma}{J^2} \tilde{T}_t^2 \quad (26)$$

Since \tilde{T} and \tilde{R}_r has been designed using a projection algorithm (bounded), from (15) and (26) we can establish that the functions $\tilde{\varphi}_{ds}, \tilde{\varphi}_{qs}, e_d, e_q$ and e_ω are bounded on $[0, \infty)$.

Consequently, from (14) it's clear that $\dot{\tilde{\varphi}}_{ds}, \dot{\tilde{\varphi}}_{qs}, \dot{e}_d, \dot{e}_q$ and \dot{e}_ω are bounded on $[0, \infty)$. So the functions $\tilde{\varphi}_{ds}, \tilde{\varphi}_{qs}, e_d, e_q$ and e_ω are uniformly continuous on $[0, \infty)$, as a result, from(13) it can be seen that $\tilde{i}_{dr}, \tilde{i}_{qr}, \tilde{i}_{dr}$ and \tilde{i}_{qr} are bounded, and the functions $\tilde{i}_{dr}, \tilde{i}_{qr}$ are also uniformly continuous on $[0, \infty)$.

The closed loop of the system (14) is determined based on (19), (21), (22) and (23) as:

$$\begin{cases} \dot{\tilde{\varphi}}_{ds} = -(\alpha + \alpha\beta M)\tilde{\varphi}_{ds} + \omega_0\tilde{\varphi}_{qs} + \alpha\beta M e_d \\ \dot{\tilde{\varphi}}_{qs} = -(\alpha + \alpha\beta M)\tilde{\varphi}_{qs} - \omega_0\tilde{\varphi}_{ds} + \alpha\beta M e_q \\ \dot{e}_d = -\left(k + \frac{\alpha\beta M}{4}\right)e_d - \frac{\tilde{R}_r}{\sigma}e_d + \frac{\tilde{R}_r}{\sigma}\tilde{\varphi}_{ds} \\ \quad + e_q e_\omega + \frac{i_{qr}^*}{\beta}e_\omega - \frac{i_{dr}^*}{\sigma\beta}\tilde{R}_r \\ \dot{e}_q = -\left(k + \frac{\alpha\beta M}{4}\right)e_q - \frac{\tilde{R}_r}{\sigma}e_q + \frac{\tilde{R}_r}{\sigma}\tilde{\varphi}_{qs} - e_d e_\omega \\ \quad - \left(\Psi^* + \frac{i_{dr}^*}{\beta}\right)e_\omega - \frac{i_{qr}^*}{\sigma\beta}\tilde{R}_r \end{cases} \quad (27)$$

We can put the last five equations of (27) in the following form:

$$\begin{aligned} \dot{x}(t) &= [A(t) + B(t)]x(t) + C(t)z(t) \\ \dot{z}(t) &= Dz(t) + Ex(t) + Fw(t) \\ \dot{w}(t) &= Gx(t) \end{aligned} \quad (28)$$

where:

$$x(t) = [\tilde{\varphi}_{ds}, \tilde{\varphi}_{qs}, e_d, e_q]^T ; z(t) = [e_\omega, \tilde{R}_r]^T ; w(t) = \tilde{T}_t$$

and

$$A(t) = \begin{pmatrix} -(\alpha + \alpha\beta M) & \omega_0 & \alpha\beta M & 0 \\ -\omega_0 & -(\alpha + \alpha\beta M) & 0 & \alpha\beta M \\ 0 & 0 & -\left(k + \frac{\alpha\beta M}{4}\right) & 0 \\ 0 & 0 & 0 & -\left(k + \frac{\alpha\beta M}{4}\right) \end{pmatrix}$$

$$B = \begin{pmatrix} 0 & 0 & 0 & 0 \\ \tilde{R}_r & 0 & -\tilde{R}_r & 0 \\ \sigma & 0 & \sigma & e_\omega \\ 0 & \tilde{R}_r & -e_\omega & -\tilde{R}_r \\ & \sigma & & \sigma \end{pmatrix} ; C = \begin{pmatrix} 0 & 0 \\ i_{qr}^* & -i_{dr}^* \\ \beta & \sigma\beta \\ -\left(\Psi^* + \frac{i_{dr}^*}{\beta}\right) & -\frac{i_{qr}^*}{\sigma\beta} \end{pmatrix}$$

$$E = \begin{pmatrix} 0 & 0 & \frac{2}{\lambda} f_1 \left(\varphi_{ds} + \frac{i_{dr}}{\beta} \right) & -\frac{2}{\lambda} f_1 \left(\varphi_{ds} + \frac{i_{dr}}{\beta} \right) \\ 0 & 0 & -f_2 \frac{i_{dr}}{\delta\sigma\beta} & -f_2 \frac{i_{qr}}{\delta\sigma\beta} \end{pmatrix}$$

$$F = \begin{pmatrix} -\frac{1}{J} \\ 0 \end{pmatrix} ; D = \begin{pmatrix} -\frac{f}{J} & 0 \end{pmatrix}$$

$$G = \begin{pmatrix} 0 & 0 & f_3 \frac{J}{\gamma} \left(\varphi_{qs} + \frac{i_{qr}}{\beta} \right) & -f_3 \frac{J}{\gamma} \left(\varphi_{ds} + \frac{i_{dr}}{\beta} \right) \end{pmatrix}$$

with $f_i, i = 1,2,3$, are bounded functions such that $0 \leq f_i \leq 1$

Since the functions $\tilde{\varphi}_{ds}, \tilde{\varphi}_{qs}, e_d, e_q, e_\omega$ are bounded, so for all $t \geq t_0$ $A(t), B(t), C(t), D(t), E(t), F(t)$ and $G(t)$ are bounded, with $\|A(t)\| \leq A_M, \|B(t)\| \leq B_M, \|C(t)\| \leq C_M, \|D(t)\| \leq D_M, \|E(t)\| \leq E_M, \|F(t)\| \leq F_M, \|G(t)\| \leq G_M$

From (15), the function $v(t)$ can be put into the following inequation:

$$\alpha_1(\|x\|^2 + \|z\|^2 + \|w\|^2) \leq v \leq \alpha_2(\|x\|^2 + \|z\|^2 + \|w\|^2) \quad (29)$$

The time derivative of $v(t)$ (26) can be written in the following way:

$$\dot{v} \leq -a_3\|x\|^2 - a_4\|w\|^2 + a_5\|w\|\|z\| \quad (30)$$

with:

$$a_3 = \min\{\alpha, k\}, a_4 = \frac{\gamma}{J^2}, a_5 = -\left(\frac{\lambda}{J} + \frac{f}{J^2}\right)$$

According to the proof of lemma 2.1 in [23], the origin $x = 0, z = 0, w = 0$ of (28) is locally exponentially stable.

4. Simulation Results

Simulation of the detailed model of 3MW DFIG-WT using the proposed adaptive nonlinear sensorless controller is performed in MATLAB/Simulink environment, the parameters and characteristics of the latter DFIG-WT along with the design parameters are given in Table 2, and Table 3, Appendix B.

The estimation and tracking performance of the adaptive sensorless controller is shown using a variable wind speed of (8.5 m/s) mean value as depicted in Figure 3. To show the robustness of the proposed adaptive sensorless controller against the aerodynamic torque and the rotor winding resistance variation the tracking performance for both the sensorless controller with [24] and without adaptation at constant wind speed (9 m/s) has been compared in Figure 4. The simulation is performed with the variation of the mechanical torque and the rotor winding resistance described by:

$$T_t = \begin{cases} T_t & \text{for } t \leq 20s \\ 0.5T_t & \text{for } t > 20s \end{cases} \quad (31)$$

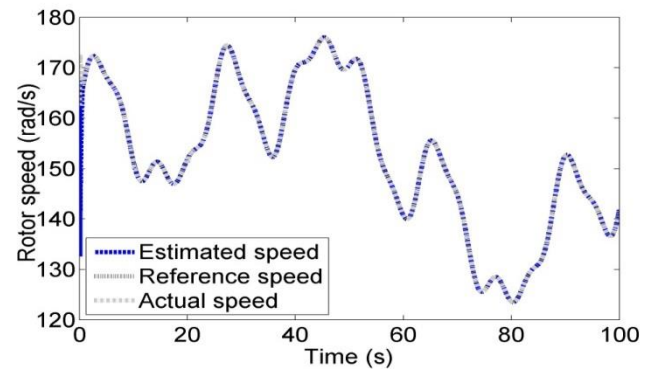
$$R_r = \begin{cases} R_r & \text{for } t \leq 10s \\ 1.5R_r & \text{for } t > 10s \end{cases} \quad (32)$$

From Figure 3 (a) and 3 (b) the actual rotor speed varies in accordance with the wind speed, which confirms the effectiveness of the MPPT. Figure 3 (c) shows a good tracking performance of the stator quadratic current. According to Figure 3(d) it can be noticed that the estimated torque recovers the applied unknown torque. Similarly, from Figure 3(e) it can be observed that the estimated rotor resistance quickly converges to its true profiles. In Figure 4 the adaptive nonlinear sensorless controller performance is shown by the comparison of the proposed adaptive sensorless and the sensorless controller proposed in [24]. From Figures 4 (a) and 4 (b) it is noted that the stator flux and the rotor speed tracking errors sustain small perturbations caused by the unknown rotor resistance and the unknown aerodynamic torque, but they converge to zero quickly as soon as the estimates of R_r , and T_t converges to their actual values. Whereas in the case of control without adaptation Figures 4 (c) and 4 (d) the rotor speed and the stator flux don't track anymore their references after variation of the rotor resistance and the aerodynamic torque.

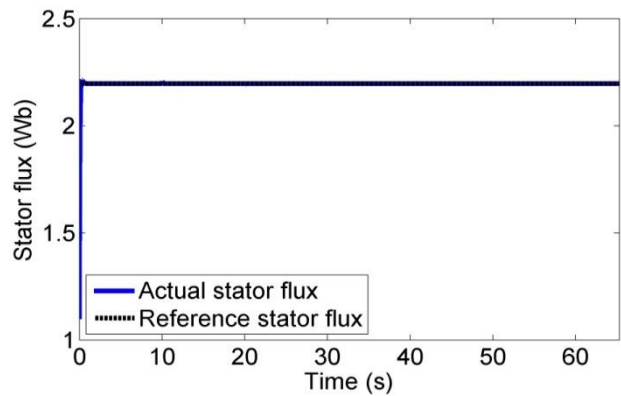
When the actual values do not correspond to their references, the closed loop system is exposed to failure, which destroys the control objectives. These results confirm the robustness of our controller regarding to the rotor resistance variation along with the aerodynamic torque.

5. Conclusion

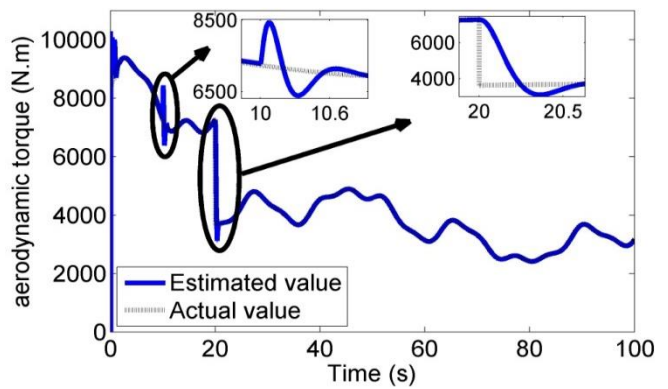
This paper presents an adaptive nonlinear sensorless controller for DFIG-WT to maximize the wind energy extracted under parametric uncertainties and unknown rotor speed. The simulation performed in Matlab/Simulink environment illustrates the good results provided by the controller regarding the good tracking capability of the rotor speed and stator flux, in addition to correct estimation of the unknown rotor speed, aerodynamic torque, and the rotor resistance. Also, the comparison result between the same controller with and without adaptation shows the effectiveness of this work.



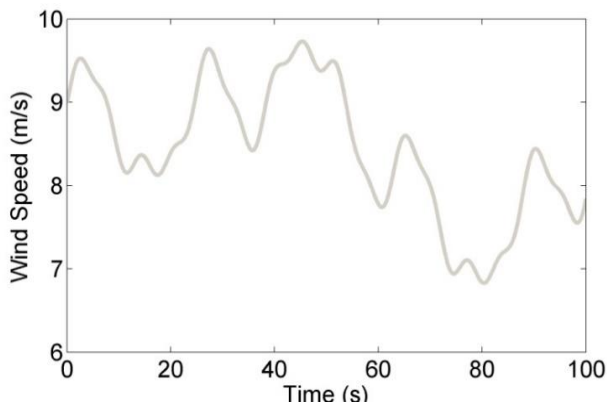
(b) Actual, Reference and estimated rotor



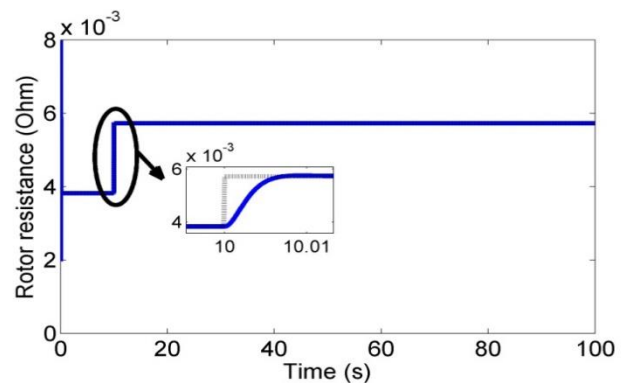
(c) The Actual and reference stator flux



(d) The aerodynamic torque and its estimate

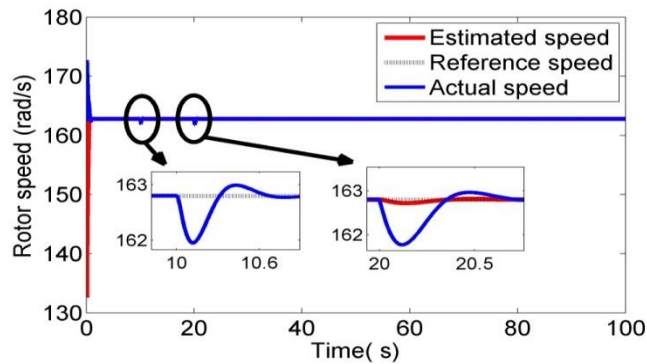


(a) Time varying wind speed

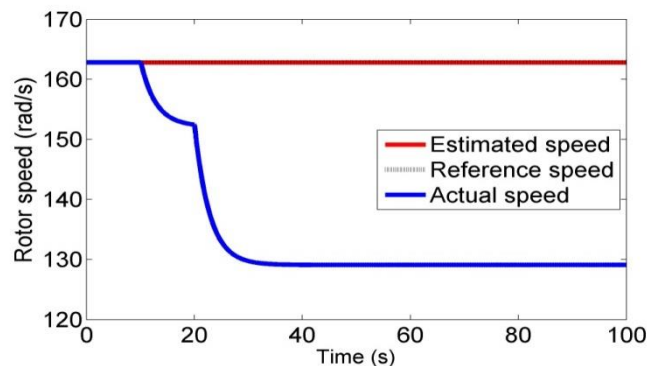


(e) The rotor resistance and its estimate

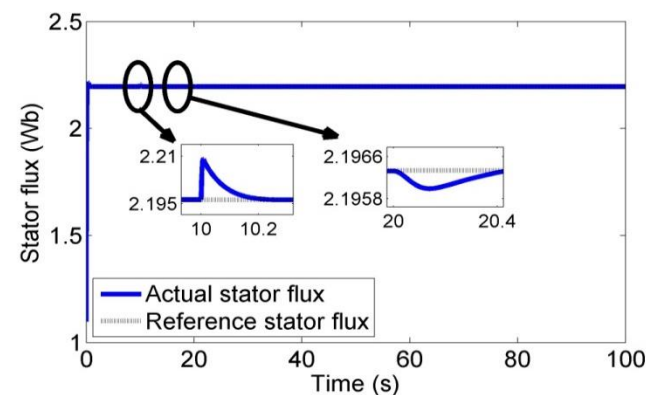
Figure 3: Comparison of tracking performance s under unknown parameters Changes occur at $t=10s \Delta R_r = 50\%$, $t=10s \Delta T_t = -50\%$ and at $t=20s$



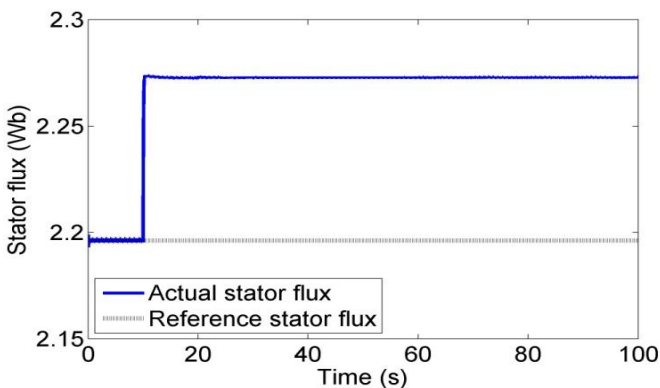
(a) Actual, Reference and estimated rotor speed with adaptation



(b) Actual, Reference and estimated rotor speed without adaptation



(c) The Actual and reference stator flux with adaptation



(d) The Actual and reference stator flux without adaptation

Figure 4: Comparison of tracking performances under unknown parameters Changes occur at $t=10s$ $\Delta R_r = 50\%$, $t=20s$ $\Delta T_f = -50\%$

References

- [1] G.M. As, "Doubly fed induction generator using back-to-back PWM converters and its application to variable- speed wind-energy generation," 1996.
- [2] S. Müller, M. Deicke, R.W. De Doncker, "Doubly fed induction generator systems for wind turbines," IEEE Industry Applications Magazine, **8**(3), 26–33, 2002, doi:10.1109/2943.999610.
- [3] G. Boroumandjazi, B. Rismanchi, R. Saidur, "Technical characteristic analysis of wind energy conversion systems for sustainable development," ENERGY CONVERSION AND MANAGEMENT, **69**, 87–94, 2013, doi:10.1016/j.enconman.2013.01.030.
- [4] A.B. Ataji, Y. Miura, T. Ise, H. Tanaka, "A Rotor-Current-Based Slip Angle Estimator for Grid-Connected Doubly Fed Induction Generator Requiring the Stator Inductance only," IEEE Transactions on Power Electronics, **32**(6), 4827–4838, 2017, doi:10.1109/TPEL.2016.2598441.
- [5] L.Y. Lu, N.F. Avila, C.C. Chu, T.W. Yeh, "Model Reference Adaptive Back-Electromotive-Force Estimators for Sensorless Control of Grid-Connected DFIGs," IEEE Transactions on Industry Applications, **54**(2), 1701–1711, 2018, doi:10.1109/TIA.2017.2765300.
- [6] M.W. Kalaga Mbukani, N. Gule, "Comparison of high-order and second-order sliding mode observer based estimators for speed sensorless control of rotor-tied DFIG systems," IET Power Electronics, **12**(12), 1–11, 2019, doi:10.1049/iet-pel.2018.6225.
- [7] R.M. Prasad, M.A. Mulla, "Position-sensorless direct torque control of grid-connected DFIG with reduced current sensors," Sadhana - Academy Proceedings in Engineering Sciences, **45**(1), 2020, doi:10.1007/s12046-020-1275-x.
- [8] H. Becheri, I.K. Bousserhane, A. Harrouz, I. Colak, K. Kayisli, "Sensorless Control of Wind Turbine Conversion Equipped with a DFIG Using MPPT Strategy," Proceedings - 2018 IEEE 18th International Conference on Power Electronics and Motion Control, PEMC 2018, (3), 605–610, 2018, doi:10.1109/EPEPEMC.2018.8522002.
- [9] E.H. Abdou, A.R. Youssef, S. Kamel, M.M. Aly, "Sensorless Wind Speed Control of 1.5 MW DFIG Wind Turbines for MPPT," 2018 20th International Middle East Power Systems Conference, MEPCON 2018 - Proceedings, 700–704, 2019, doi:10.1109/MEPCON.2018.8635209.
- [10] B. Yang, L. Jiang, L. Wang, W. Yao, Q.H. Wu, "Nonlinear maximum power point tracking control and modal analysis of DFIG based wind turbine," International Journal of Electrical Power & Energy Systems, **74**, 429–436, 2016, doi:10.1016/j.ijepes.2015.07.036.
- [11] G.E.-P. and R.E.-P. López-García, F. Beltran-Carbajal, "A Review of RFO Induction Motor Parameter Estimation Techniques," **18**(2), 271–283, 2003.
- [12] J.M. Mauricio, A.E. Leon, A. Gomez-Exposito, J.A. Solsona, "An Adaptive Nonlinear Controller for DFIM-Based Wind Energy Conversion Systems," IEEE Transactions on Energy Conversion, **23**(4), 1025–1035, 2008.
- [13] A. Susperregui, I. Lizarraga, J. Jugo, G. Tapia, "Automated control of doubly fed induction generator integrating sensorless parameter estimation and grid synchronisation," IET Renewable Power Generation, **8**(1), 76–89, 2014, doi:10.1049/iet-rpg.2013.0045.
- [14] R. Ourhdir, M. Rachidi, "Adaptive input-output feedback linearization control of doubly-fed induction machine in wind power generation," International Review of Automatic Control, **12**(1), 11–20, 2019, doi:10.15866/ireaco.v12i1.15619.
- [15] J.M. Pinar Pérez, F.P. García Márquez, A. Tobias, M. Papaelias, "Wind turbine reliability analysis," Renewable and Sustainable Energy Reviews, **23**(March), 463–472, 2013, doi:10.1016/j.rser.2013.03.018.
- [16] X. Jin, W. Ju, Z. Zhang, L. Guo, X. Yang, "System safety analysis of large wind turbines," Renewable and Sustainable Energy Reviews, **56**, 1293–1307, 2016, doi:10.1016/j.rser.2015.12.016.
- [17] F. Liu, D. Li, P. Li, Y. Song, "Quadratic Optimal Tracking Control of Wind Turbine Systems," IFAC-PapersOnLine, **48**(28), 502–507, 2015, doi:10.1016/j.ifacol.2015.12.178.
- [18] S. Heier, GRID INTEGRATION OF WIND ENERGY GRID INTEGRATION OF WIND ENERGY ONSHORE AND OFFSHORE.
- [19] I. Press, L. Shafer, G.W. Arnold, D. Jacobson, ANALYSIS OF ELECTRIC MACHINERY AND DRIVE SYSTEMS.
- [20] G. Abad, J. López, M.A. Rodríguez, L. Marroyo, G. Iwanski, Doubly Fed Induction Machine: Modeling and Control for Wind Energy Generation, 2011, doi:10.1002/9781118104965.
- [21] R. Marino, P. Tomei, C.M. Verrelli, Induction Motor Control Design, 2010, doi:10.1007/978-1-84996-284-1.
- [22] L. Praly, "Adaptive Nonlinear Regulation: Estimation from the Lyapunov Equation," IEEE Transactions on Automatic Control, **37**(6), 729–740, 1992,

doi:10.1109/9.256328.

- [23] R. Marino, G.L. Santosuosso, P. Tomei, "Robust adaptive observers for nonlinear systems with bounded disturbances," IEEE Transactions on Automatic Control, **46**(6), 967–972, 2001, doi:10.1109/9.928609.
- [24] R. Ourhdir, M. Rachidi, "Nonlinear sensorless control of doubly fed induction generator in wind power generation," 2020 1st International Conference on Innovative Research in Applied Science, Engineering and Technology, IRASET 2020, 2(1), 2020, doi:10.1109/IRASET48871.2020.9091997.

Appendix A. Frame transformation and u_{ds} derivative

The direct and quadratic components of the stator voltage in the (d, q) reference frame can be expressed as follows:

$$\begin{pmatrix} u_{ds} \\ u_{qs} \end{pmatrix} = \begin{pmatrix} \cos \theta_0(t) & \sin \theta_0(t) \\ -\sin \theta_0(t) & \cos \theta_0(t) \end{pmatrix} \begin{pmatrix} u_{\alpha s} \\ u_{\beta s} \end{pmatrix} \quad (A.1)$$

where (α, β) stand for the fixed reference frame and θ_0 the electrical angle of the (d, q) rotating reference frame to the (α, β) one, see Figure 2. The components of the stator voltage in (α, β) are:

$$\begin{pmatrix} u_{\alpha s} \\ u_{\beta s} \end{pmatrix} = \underbrace{\sqrt{\frac{2}{3}} \begin{pmatrix} 1 & -\frac{1}{2} & -\frac{1}{2} \\ 0 & \sqrt{\frac{3}{2}} & -\sqrt{\frac{3}{2}} \end{pmatrix}}_{\tilde{T}} \begin{pmatrix} u_{as} \\ u_{bs} \\ u_{cs} \end{pmatrix} \quad (A.2)$$

In which T is the Concordia matrix transformation, and u_{as}, u_{bs} and u_{cs} are the 3-phases stator voltage giving by :

$$\begin{pmatrix} u_{as} \\ u_{bs} \\ u_{cs} \end{pmatrix} = V_m \begin{pmatrix} \sin(\omega_s t) \\ \sin(\omega_s t - \frac{2\pi}{3}) \\ \sin(\omega_s t + \frac{2\pi}{3}) \end{pmatrix} \quad (A.3)$$

Using the conventional derivative proprieties for scalar, vector and matrix, we can obtain the direct stator voltage component derivative $\frac{du_{ds}}{dt}$ used in (14). From (A.1) the expression of the direct stator voltage is:

$$u_{ds} = (\cos \theta_0(t) \quad \sin \theta_0(t)) \begin{pmatrix} u_{\alpha s} \\ u_{\beta s} \end{pmatrix}$$

From (A.2), (A.3) and (10), the derivative of u_{ds} is given by:

$$\begin{aligned} \frac{du_{sd}}{dt} &= [u_{as} \quad u_{bs} \quad u_{cs}] \tilde{T}^T \frac{u_{qs} + \alpha M i_{qr}^*}{\Psi^*} \begin{bmatrix} -\sin \theta_0(t) \\ \cos \theta_0(t) \end{bmatrix} \\ &+ [\cos \theta_0(t) \quad \sin \theta_0(t)] \tilde{T} \omega_s V_m \begin{bmatrix} \sin(\omega_s t + \frac{\pi}{2}) \\ \sin(\omega_s t - \frac{\pi}{6}) \\ \sin(\omega_s t - \frac{5\pi}{6}) \end{bmatrix} \end{aligned} \quad (A.4)$$

$$\cos \theta_0(t) = \frac{\varphi_{\alpha s}}{\sqrt{\varphi_{\alpha s}^2 + \varphi_{\beta s}^2}} \quad \text{and} \quad \sin \theta_0(t) = \frac{\varphi_{\beta s}}{\sqrt{\varphi_{\alpha s}^2 + \varphi_{\beta s}^2}}$$

Appendix B. characteristics/parameters of 3 MW DFIG-WT and the adaptive sensorless controller

Table 2: Characteristics and parameters of DFIG-WT

Parameter	Definition	Value
Induction generator		
P_{rat}	Rated power	3 MW
U	Rated stator voltage	690 V
ω_s	Stator angular frequency	314 rad/s
p	Number of pole pairs	2
R_r	Rotor winding resistance	0.00382 Ω
R_s	Stator winding resistance	0.00297 Ω
L_r	Rotor inductance	0.0122 H
L_s	Stator inductance	0.0122 H
M	Mutual inductance	0.01212 H
Wind Turbine		
R	Blade Radius	45 m
G	Gearbox ratio	100
$C_{p \max}$	Maximal Power coefficient	0.48
λ_{opt}	Optimal Tip Speed Ratio(TSR)	8.14
Generator and Turbine		
J	Moment of inertia	254 kg.m ²
f	Dumping coefficient	0.24
f_r	grid frequency	50 Hz
U	grid voltage	690 V

Table 3: parameters of the adaptive sensorless controller

Parameter	Value
k	6000
k_ω	100
δ	70000
γ	0.0098
T_{IM}	10000
R_{rm}	$0.5R_r$
R_{rM}	$2R_r$
ε_1	$0.001R_r$
ε_2	5